



**HAL**  
open science

# Spontaneous generation, enhanced propagation and optical imprinting of quantized vortices and dark solitons in a polariton superfluid: Towards the control of quantum turbulence(a)

A Maitre, F Claude, G Lerario, S Koniakhin, S Pigeon, Dmitry Solnyshkov, Guillaume Malpuech, Q Glorieux, E Giacobino, A Bramati

## ► To cite this version:

A Maitre, F Claude, G Lerario, S Koniakhin, S Pigeon, et al.. Spontaneous generation, enhanced propagation and optical imprinting of quantized vortices and dark solitons in a polariton superfluid: Towards the control of quantum turbulence(a). EPL - Europhysics Letters, 2021, 134, pp.24004. 10.1209/0295-5075/134/24004 . hal-03705442

**HAL Id: hal-03705442**

**<https://uca.hal.science/hal-03705442v1>**

Submitted on 5 Jul 2022

**HAL** is a multi-disciplinary open access archive for the deposit and dissemination of scientific research documents, whether they are published or not. The documents may come from teaching and research institutions in France or abroad, or from public or private research centers.

L'archive ouverte pluridisciplinaire **HAL**, est destinée au dépôt et à la diffusion de documents scientifiques de niveau recherche, publiés ou non, émanant des établissements d'enseignement et de recherche français ou étrangers, des laboratoires publics ou privés.



Distributed under a Creative Commons Attribution 4.0 International License

LETTER

# Spontaneous generation, enhanced propagation and optical imprinting of quantized vortices and dark solitons in a polariton superfluid: Towards the control of quantum turbulence<sup>(a)</sup>

To cite this article: A. Maître *et al* 2021 *EPL* **134** 24004


View the [article online](#) for updates and enhancements.

## You may also like

- [Quantum, or classical turbulence?](#)  
M. La Mantia and L. Skrbek
- [Turbulence in quantum fluids](#)  
Makoto Tsubota
- [Quantum turbulence in atomic Bose-Einstein condensates](#)  
A J Allen, N G Parker, N P Proukakis et al.

## Focus Article

# Spontaneous generation, enhanced propagation and optical imprinting of quantized vortices and dark solitons in a polariton superfluid: Towards the control of quantum turbulence<sup>(a)</sup>

A. MAÎTRE<sup>1</sup>, F. CLAUDE<sup>1</sup>, G. LERARIO<sup>1</sup>, S. KONIAKHIN<sup>2</sup>, S. PIGEON<sup>1</sup>, D. SOLNYSHKOV<sup>2</sup>, G. MALPUECH<sup>2</sup>,  
Q. GLORIEUX<sup>1</sup>, E. GIACOBINO<sup>1</sup> and A. BRAMATI<sup>1(b)</sup> 

<sup>1</sup> *Laboratoire Kastler Brossel, Sorbonne Université, CNRS, ENS-Université PSL, Collège de France - Paris, France*

<sup>2</sup> *Institut Pascal, PHOTON-N2, Université Clermont Auvergne, CNRS, SIGMA-Clermont  
Clermont-Ferrand, France*

received 15 February 2021; accepted in final form 26 May 2021  
published online 12 July 2021

**Abstract** – In resonantly pumped polariton superfluids we recently explored a new regime based on the bistability of the polariton system to enhance the propagation of polariton fluids up to macroscopic distances. This technique together with an all-optical imprinting method allowed the generation and control of various topological excitations such as quantized vortices and dark solitons. The flexibility and scalability of the new experimental scheme opens the way to the systematic study of quantum turbulence in driven dissipative quantum fluids of light. In this article we review the main results and discuss the most promising future research directions.

focus article

Copyright © 2021 EPLA

**Introduction.** – Exciton-polaritons are half-light half-matter quasi-particles coming from the strong coupling between excitons and photons in semiconductor microcavities [1]. They inherit specific properties from their components: a very light mass coming from the photon component and strong mutual interactions from their excitonic nature.

In the last decade these systems have demonstrated to be an ideal playground for the study of out-of-equilibrium condensates and 2D quantum fluid hydrodynamics [2]. In particular, the creation of polariton fluids via an all-optical excitation enabling a full control of the speed of polariton flows allowed the hydrodynamic generation of a rich variety of topological excitations, ranging from quantized vortices to dark solitons, via the interaction of a supersonic polariton wavepacket with a structural defect [3–9]. Pulsed resonant excitation as well as CW resonant pumping have been used. However, both configurations exhibit the same fundamental limitation: the polariton density strongly decays along the propagation due to the short polariton lifetime. As a result, the propagation distances

accessible in these early experiments are quite short, strongly limiting the study of the dynamics of the topological excitations.

In a series of recent articles, devoted to the deep study of the properties of the bistability exhibited by the polariton systems under resonant pumping, we investigated a new configuration and demonstrated that in the bistable regime it is possible to get rid of the polariton density decay and to generate a superfluid flow propagating for macroscopic distances, typically one order of magnitude longer than the previous observations. Remarkably, in the bistable regime the topological excitations can be generated and their propagation sustained and strongly enhanced far beyond the polariton free propagation length. Moreover, we implemented an all-optical imprinting technique which allowed us to generate in a fully controlled way dark soliton pairs in different regimes and to study their stability against the onset of the snake instabilities [10]. The observation of the breaking of dark solitons in vortex streets illustrates the high potential of this method for the systematic study of the quantum turbulence in polariton quantum fluids.

**Theoretical model.** – The standard way to describe the dynamics of a resonantly driven polariton fluid is to

<sup>(a)</sup>Contribution to the Focus Issue *Turbulent Regimes in Bose-Einstein Condensates* edited by Alessandra Lanotte, Iacopo Carusotto and Alberto Bramati.

<sup>(b)</sup>E-mail: alberto.bramati@lkb.upmc.fr (corresponding author)

use a generalized Gross-Pitaevskii equation for the polariton field [2].

In particular, for the lower polariton branch, it reads as follows:

$$i\hbar\frac{\partial}{\partial t}\Psi = \left(\hbar\omega_{LP} - \frac{\hbar^2}{2m}\nabla_{\mathbf{r}}^2 + V - i\hbar\gamma + \hbar gn\right)\Psi + i\hbar\eta F_p \quad (1)$$

with  $\hbar\omega_{LP}$  the energy of the lower polariton,  $m$  the effective mass of the lower polariton, which is given by the second-order derivative of its dispersion curve, and is of the order of  $10^{-5}$  the mass of the electron,  $V$  the external potential felt by the lower polaritons,  $\gamma$  is the decay rate of the polaritons,  $g$  the interaction constant between the lower polaritons in the same modes and  $\hbar\eta$  is the coupling coefficient of the pump field to the polariton field.

This equation is very similar to the standard Gross-Pitaevskii which describes the atomic BECs, except for the loss term  $-i\hbar\gamma$  and the pump term  $F_p(\mathbf{r}, t)$ . The losses need to be continuously compensated: differently from atomic BECs, our system is out of equilibrium.

Let us now focus on the mean-field stationary solutions of eq. (1) in the homogeneous case, *i.e.*, for an external potential equal to zero. The system is driven by the pump field  $F_p(\mathbf{r}, t) = F_p(\mathbf{r})e^{i(\mathbf{k}_p\mathbf{r} - \omega_p t)}$ . Therefore, the solutions can be written as  $\Psi(\mathbf{r}, t) = \Psi_0(\mathbf{r})e^{i(\mathbf{k}_p\mathbf{r} - \omega_p t)}$ . It results in the mean field stationary equation:

$$\left(\hbar(\omega_{LP} - \omega_p) + \frac{\hbar^2\mathbf{k}_p^2}{2m} - i\hbar\gamma + \hbar gn_0\right)\Psi_0 + i\hbar\eta F_p = 0. \quad (2)$$

This equation is responsible for the bistability phenomenon observed in polariton system and induced by a quasi-resonant pumping [11].

A very specific behaviour of the system when it is excited in the bistable range was pointed out in [12]: the authors suggested to use the optical bistability of an exciton-polariton system to enhance the propagation of the polariton superfluid. In particular, the use of two different beams, simultaneously exciting the microcavity, can enable the generation, over a macroscopic scale, of a high-density, bistable, polariton fluid.

Let us consider two driving fields, with the same frequency  $\omega_p$  and the same in-plane wave vector  $\mathbf{k}_p$ . The first one, called the seed, is localized in space and has a high intensity. It thus produces a nonlinear superfluid above the bistability cycle. The second field is the support, ideally an infinitely extended constant field, stationary in time and homogeneous in space. Its intensity is weaker than the intensity of the seed one, and it is placed inside the bistability cycle. The presence of the support field has a strong impact on the total polariton density: its high density created at the seed location is maintained without any decrease all over the region where the support is present.

### Slightly supersonic flow: vortex stream generation.

– In this section we show that in polariton fluids in the bistable regime it is possible to generate topological excitations propagating for macroscopic distances [13]. The different hydrodynamic regimes of a polariton fluid and their effects on the generation of topological excitations have been previously studied in the case of direct injection [14,15] and for a single intense and localized pump, placed upstream of a structural defect [6,16]. The presence of the defect creates turbulence along the flow, which evolves differently depending on the ratio between the group velocity of the fluid  $v_f = (\hbar k_p)/m$  and the sound velocity  $c_s = \sqrt{gn_0/m}$ , *i.e.*, the Mach number of the system:  $M = v_f/c_s$ . Both these quantities and consequently the Mach number can be controlled in the experiment by setting the transverse wave vector and the intensity of the excitation beam. Although, depending on the size and shape of the defect, the superfluidity breaking can occur at a critical velocity which differs from the speed of sound, still the transition between the superfluid regime and the turbulent one, in which quantized vortices are generated, is well captured by the Mach number. Increasing the Mach number induces an increase in the emission rate of the vortices, which will finally merge together in a pair of dark solitons for a Mach number close to 1 or higher.

The idea here is to use the seed-support configuration previously described to generate topological excitations, such as dark solitons and quantized vortex-antivortex pairs with enhanced propagation distances.

To numerically reproduce the effect of a cavity structural defect, a large potential photonic barrier is introduced ( $V \neq 0$ ). The seed is placed upstream to it, localized and with a fixed intensity above the bistability cycle.

Time-resolved numerical simulations have been made in order to precisely locate the vortex-antivortex pairs, however as the experiment is in continuous wave excitation, time-integrated numerical simulations were also performed. Figure 1 shows the comparison between a snapshot image on the left, and, with the same parameters, an image with 1 ms integration time, on the right. Vortex and antivortex have opposite circulation, and are spotted by red and blue dots, respectively. A time average flow of vortex pairs appears as a thick line of lower density, the dip height of which is proportional to the vortex density.

The experimental setup is displayed in fig. 2 [13]. The laser source is a CW Ti-sapphire laser. It is split into the main beam and the reference beam, used to realize interferograms and get information on the phase. The main beam is split again to generate the seed and the support beams. The seed is focused on the sample into a spot with a 30 microns diameter, for an intensity  $I_r = 10.6 \text{ W/mm}^2$ . On the other hand, the support is shaped by two cylindrical lenses in an elliptical spot of 400 microns length, elongated in the  $y$ -direction with an intensity of  $5.8 \text{ W/mm}^2$ .

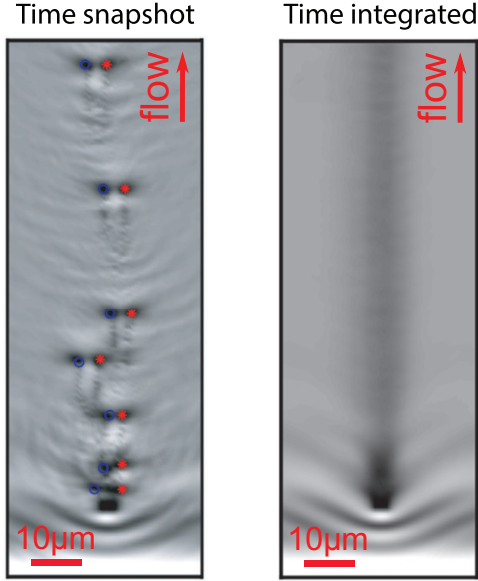


Fig. 1: Numerical simulations. On the left, the time snapshot shows the position of vortex and antivortex flowing in the wake of the defect. On the right, the time integrated image results in a thick shadow along the flow. Adapted from [12].

The inset of fig. 2 gives a representation of the relative position of the beams. The real space detection gives access to the polariton density in the plane of the cavity. The reference beam interferes with the signal of the cavity and the resulting interferogram is used to reconstruct the phase map. The other parameters of the excitation such as the wave vector in the transverse plane and the initial detuning with respect to the lower polariton branch, are coming from the momentum space data, acquired via a spectrometer.

The sample under investigation is a GaAs/AlGaAs microcavity with 21/24 (front/back) layers of DBR and  $\text{In}_{0.04}\text{Ga}_{0.96}\text{As}$  quantum wells at each of the three antinodes of the confined electromagnetic field [17]. A small wedge is inserted between the Bragg mirrors during the fabrication process allowing to precisely select the cavity-exciton detuning. The half Rabi splitting is 2.55 meV. The polariton mass, extracted from the dispersion, is  $7 \cdot 10^{-5}$  free electron mass. The polariton lifetime is about 14 ps. The experiments are performed in a liquid helium cryostat at cryogenic temperature in transmission configuration.

The results when both seed and support are sent together are shown in fig. 3. They hit a structural defect whose size of the order of  $10 \mu\text{m}$  is larger than the healing length of the fluid,  $\xi$ , defined as [2]  $\xi = \frac{\hbar}{\sqrt{2m\hbar gn}}$  with  $m$  the effective polariton mass and the product  $gn$  the polariton interaction energy. In our experimental conditions the healing length is typically around  $5 \mu\text{m}$ . The speed of fluid is  $v_f = 0.9 \mu\text{m}/\text{ps}$  and the speed of sound is  $c_s = 0.8 \mu\text{m}/\text{ps}$ . This sets the Mach number  $M = 1.1$

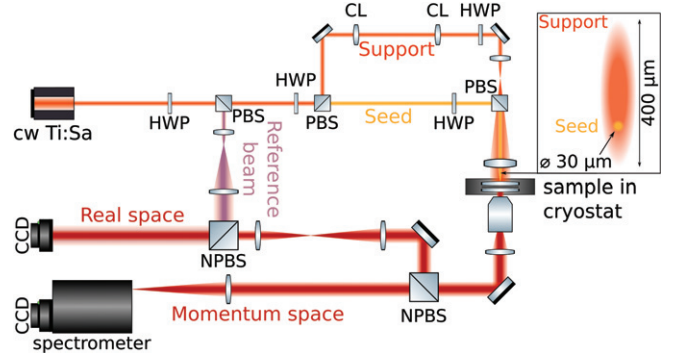


Fig. 2: Experimental setup. The CW Ti:Sa laser beam is split into three using half waveplates (HWP) and polarizing beam-splitter (PBS). A reference beam, in light red, is set aside for interferogram on the detection part; the focused seed beam is in yellow, the elongated support beam in orange. The positions of seed and the support are shown in the inset. The detection is done in real space (density and phase maps) and in momentum space through the spectrometer. Adapted from [13].

As predicted, a shadow appears in the wake of the defect, which corresponds very well to the time-integrated image numerically calculated and presented in fig. 1. The pairs of vortex-antivortex are generated around the defect and follow the flow, leading to a decrease of density along their propagation path on the time-integrated image.

To confirm that this shadow is indeed due to the presence of vortices, an interferogram has been realized as well as a visibility map, defined as  $Vis(r) = (I_{max}(r) - I_{min}(r)) / (I_{max}(r) + I_{min}(r))$ . They are displayed in figs. 3(b) and (c). As the vortices are moving along the flow, one cannot expect to observe forks, the typical signature of vortices, due to the low time resolution of the detection (the integration time is typically of few milliseconds, while the flow speed is about  $1 \mu\text{m}/\text{ps}$ ). However, the presence of the vortices is visible on the phase map as a blur of the fringes along their path.

Moreover, the shadow and the phase variations coincide with a dip in visibility, confirming its attribution to the vortex stream. The full control over the speed of fluid and its propagation distance allows us to generate and propagate quantized vortices, as demonstrated in fig. 3. The proof of principle uses here a single structural defect; however the technique is easily scalable by using multiple optically generated obstacles [18] hit by the fluid and can be employed to investigate polariton fluids in deep quantum turbulent regimes.

**Deeply supersonic flow: parallel dark soliton pair generation.** – In this section we show how to generate stable dark solitons propagating for long distances in the polariton fluid [19]. In order to study the generation of solitons, the supersonic configuration is investigated. According to previous studies in polaritons superfluid [6], high Mach numbers allow for the generation of dark



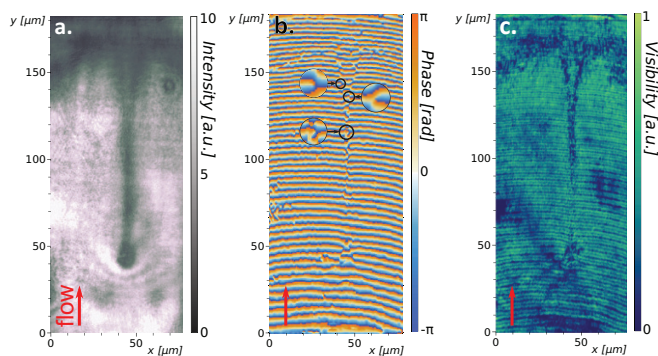


Fig. 3: Vortex stream generation. (a) Time-integrated density map of a flow of vortex pairs generated in the wake of a defect. (b) Interferogram of the previous image, showing phase irregularities along the vortices propagation. (c) Visibility map extracted from the interferogram, displaying a lower visibility along the vortex stream. Adapted from [13].

solitons. However, the system configuration, without the support beam, did not allow for long propagation: the solitons, generated in the wake of a defect, could only be observed for short distances (around 30 micrometers), limited by the exponential decay of the polariton density due to the finite polariton lifetime.

The goal here is to use the configuration of seed-support excitation to generate dark solitons propagating over long distances and to enable the study of their hydrodynamic behaviour.

The setup of this experiment is similar to the previous one for the vortex generation, with two co-propagating beams sent to the cavity: the seed, localized and intense, and the support, extended and with an intensity within the bistability cycle. The seed is placed upstream of a structural defect

To generate dark solitons in its wake, the in-plane wave vector is chosen to be high ( $k = 1.2 \mu\text{m}^{-1}$ ) in order to ensure a high velocity of the fluid: in this case,  $v_f = 1.52 \mu\text{m}/\text{ps}$ . The speed of sound is measured to be  $c_s = 0.4 \mu\text{m}/\text{ps}$ : the supersonic conditions are reached, with the Mach number  $M = 3.8$ . Figure 4 presents the observation of a spontaneous generation of dark solitons in the wake of a defect: intensity on the left and interferogram on the right. The propagation length is greatly enhanced. The scale bar illustrates 20 microns: the solitons are sustained for more than a hundred microns, one order of magnitude more than previously reported.

Moreover the solitons have a surprising behaviour. They are generated close to the defect and propagate away from each other for a few microns; eventually, they reach an equilibrium separation distance of about 8 microns, align and stay parallel as long as they are sustained. The observation of such a bound state of dark solitons is quite unexpected as solitons have repulsive interactions [20]. The observed solitons are fully dark: the intensity dip goes to zero and the phase jump across the solitons is nearly  $\pi$  all

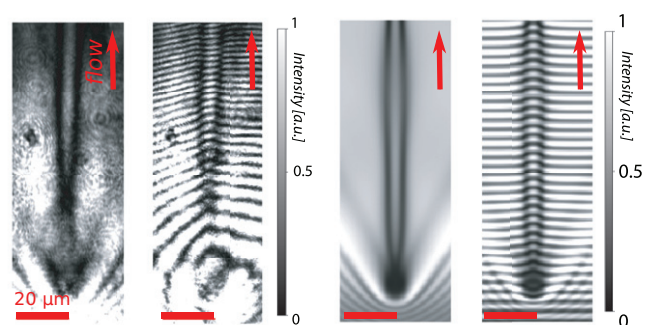


Fig. 4: Spontaneous generation of parallel dark solitons. From left to right: experimental polariton density and interferogram; corresponding numerical simulations. Adapted from [19].

along the propagation, confirming their transverse velocity is close to zero.

The results of the numerical simulations are presented in fig. 4 and show an excellent agreement with the experimental data. This model allows to show that the driving field compensates for the soliton repulsion.

#### All-optical imprinting of dark soliton molecules in a polariton superfluid.

– We present here an all-optical technique allowing to imprint dark solitons in a polariton superfluid [21]. We described in the previous section how to use the bistable behaviour of the polariton system to enhance the propagation length of a polariton superfluid, simultaneously getting rid of the phase constraint of the pump. This allowed us to observe the spontaneous generation of quantized vortices and dark solitons and their propagation for over a hundred microns. However, their generation was not fully controlled, since it depends on parameters out of reach; in particular, the presence of a structural defect is necessary to induce the turbulence leading to the topological excitations [13,19].

The goal in this section is to show how to overcome this limitation and to be able to generate solitons on demand. This is realized by imprinting a phase modulation on the system, leading to the formation of dark solitons that can evolve freely on the nonlinear fluid [21].

As the solitons induce a phase jump on the system, their implementation can be done by engineering the phase of the excitation. To do so, we use a Spatial Light Modulator, a liquid-crystal-based device that can shape the wavefront of an incident light beam. The phase modulation induced by dark solitons is a phase jump of  $\pi$ : the phase profile corresponding to a pair of dark solitons is thus an elongated region  $\pi$ -shifted compared to the background beam.

The experimental setup is sketched in fig. 5. The laser source is a CW Ti:sapphire, and its spot is elongated in the  $y$ -direction by two cylindrical lenses (CL). The beam is then split in two by a polarizing beam splitter (PBS) preceded by a half-wave plate (HWP), which allows for a precise control of the power sent in each arm. The phase

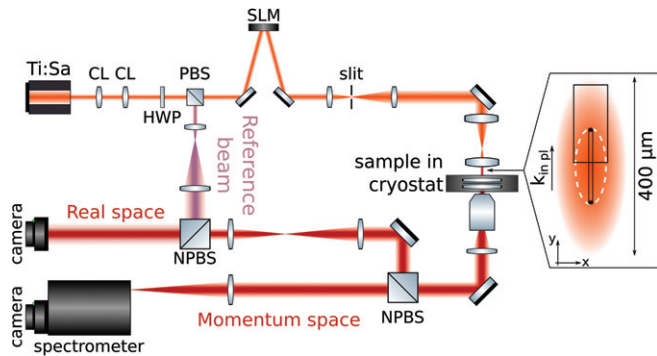


Fig. 5: Experimental setup. The excitation beam is designed by the SLM and filtered through the slit. The inset illustrates the beam configuration: the solitonic pattern is in the center, where the intensity is above the bistability limit, located at the white dashed line. The detection field of view is delimited by the black rectangle. Adapted from [21].

front of the main beam is shaped by the SLM, then is filtered by the slit to smooth the phase jump in the direction of the flow. This beam is sent collimated to the cavity, so that the phase jumps are well defined onto the sample. The inset illustrates the excitation beam configuration on the sample: the solitonic pattern is placed in the center, where the intensity is above the bistability limit, delimited by the white dashed line. The beam enters the cavity with an appropriate in-plane wave vector that gives an upward flow to the polaritons. The black rectangle is the detection field of view: it is shifted on top of the illuminated region to observe the solitons free propagation through the bistable area. As usual, the detection is done in both real and momentum space. The real space gives the intensity map of the cavity plan, as well as information on the phase pattern through the interference with the reference beam previously separated from the laser beam. The experimental parameters such as the wave vector in the transverse plane and the initial detuning with respect to the lower polariton branch are measured with precision using the momentum space images. The experimental conditions of fig. 6 are the following: the speed of fluid is  $v_f = 1.35 \mu\text{m}/\text{ps}$ , the speed of sound is measured to be  $c_s = 0.31 \mu\text{m}/\text{ps}$ , with the Mach number  $M = 4.35$ .

The essential role of the bistability in the propagation of the solitons is explained in fig. 6. Figure 6(a) shows the S shape of the bistability curve and the three associated intensity regions: below the cycle, the low-density region in grey, denoted as LD; above the cycle, the high-density region highlighted in yellow and denoted as HD; and the bistable cycle left blank. Note that the property of the fluid to be in the bistable region only depends on its density. Then the bistable region can be obtained with one beam only, properly shaped by the SLM, without the need of the support beam.

In fig. 6(b) the phase pattern designed by the SLM is plotted with the same field of view as the detection: we

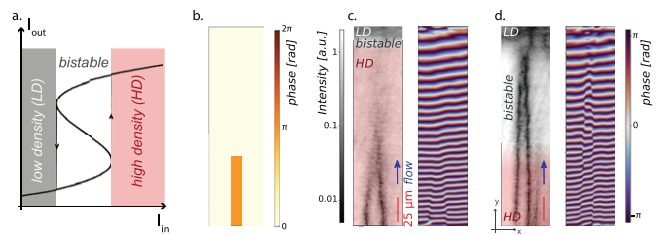


Fig. 6: Impression of dark parallel solitons. (a) Theoretical bistability profile. (b) SLM phase pattern with the same field of view as the detection. (c) High power density and phase maps. (d) Same configuration as (c) at lower power. Adapted from [21].

can see that the phase modulation is only present on the bottom part of the image. Figures 6(c) and (d) are realized in the exact same conditions except for the total intensity of the excitation. In fig. 6(c), the total laser power is high, which puts almost all the illuminated area above the bistability cycle: the yellow HD region covers the major part of the picture. In the high-density region the properties of the fluid are fixed by the pump: this area is therefore a replica of the driving pump field. Indeed, the solitons are imprinted only in the bottom part of the picture, while on top, the phase and the intensity of the pump beam are flat.

The images in fig. 6(d) are obtained by starting from same laser intensity as in fig. 6(c) and then gradually decreasing the input intensity. The bistable region expands toward the center of the beam, and eventually reaches the top part of the imprinted solitons. The solitons then propagate through the bistable region, even though the region between the solitons is out of phase with the driving field. The propagation is sustained as long as the system is in the bistable regime.

These measurements clearly confirm the necessity to be in the bistable regime (namely inside the bistability cycle) to achieve the free propagation of dark solitons in a resonantly pumped polariton fluid.

To illustrate the scalability of the imprinting method, we show in fig. 7(a) a double pair of solitons. Figure 7(a) shows a scheme of the SLM phase pattern. It represents the top part of the beam, coinciding with the corresponding detection pictures, plotted in figs. 7(b) and (c) and showing the density map and the interferogram, respectively.

The double pair of solitons is realized by sending two rectangular shapes in phase opposition with the background thanks to the SLM. The imprinted phase pattern is designed so that each of the four solitons is equidistant from its neighbor (yellow part of fig. 7(b)).

**Snake instabilities, soliton breaking and vortex streets.** – In this section we focus on the study of the stability of solitonic patterns [22]. In the experiments described in the previous section we studied stable solitons and for this purpose we chose to work in a supersonic

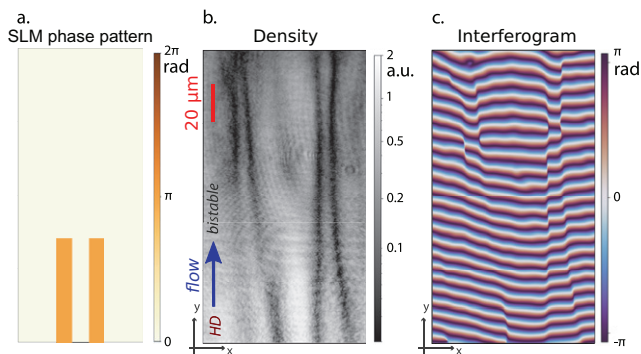


Fig. 7: Four solitons imprinting. (a) SLM phase pattern corresponding to the detection region. (b) Density map of the fluid. The two solitons pairs are imprinted on the yellow region and propagate through the bistable white one. (c) Interferogram of the fluid. The phase jump propagates with the solitons. Adapted from [21].

regime with high-speed polariton flows [23]. However, the flexibility of the imprinting technique and the full control of the fluid velocity that can be achieved, easily allow one to imprint dark solitons on polariton fluids with deeply subsonic velocities. In these conditions, it is well known that dark solitons are unstable against the snake instabilities and break into quantum vortex-antivortex pairs, a behaviour which is a quantum analog of the classical von Kármán vortex street [24]. Therefore this technique can be exploited for the study of quantum turbulence.

As an example of such possibilities, in this section we investigate a new configuration to generate solitonic patterns within a static polariton fluid. It uses a transverse confinement within an intensity channel to create a pair of dark solitons, which decays into vortex streets due to the disorder of the system. We observe the soliton snake instability leading to the formation of symmetric arrays of vortex streets, which are frozen by the pump-induced confining potential allowing their direct observation and a quantitative study of the onset of the instabilities.

The setup used for this experiment is quite similar to the one of the soliton imprinting, presented in the previous section. Two main differences have yet to be noticed. First of all, to facilitate the development of the instabilities, the experiment needs a static fluid: the excitation is therefore sent at normal incidence, and the in-plane wave vector is zero. The intensities inside and outside the channel are denoted  $S$  and  $P$ , respectively. Then, the 1D elongated channels which confine the dark solitons are created by shaping the intensity of the excitation beam, while its phase is not modulated anymore.

We consider a channel with both the ends closed by high-density walls (fig. 8). The channel width of  $23\ \mu\text{m}$  is chosen in order to generate a single dark soliton pair, which evolves toward a stationary frozen vortex street due to the snake instability.

In fig. 8, panel (a) shows the measured intensity and phase distributions in the channel for increasing ratios

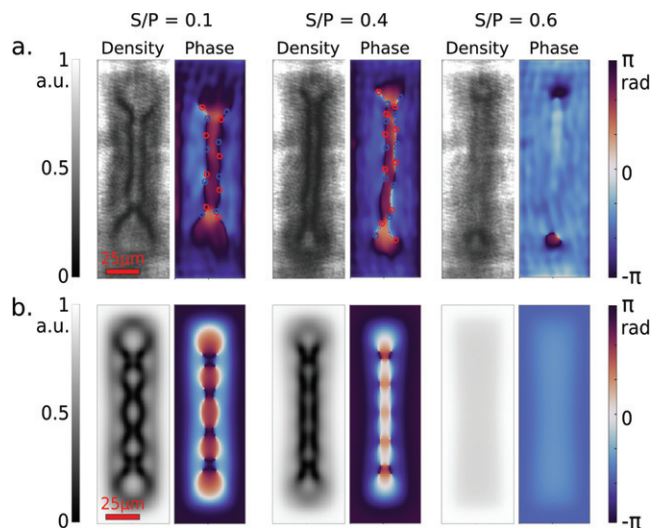


Fig. 8: Panel (a): experimental fluid density and phase maps for a channel with length and width respectively  $l = 150\ \mu\text{m}$ ,  $L = 23\ \mu\text{m}$ ; the ratio  $S/P$  increases from left to right. Panel (b): corresponding numerical simulations. Adapted from [22].

$S/P$ . Panel (b) shows the corresponding numerical simulations obtained by solving the system of coupled equations. A symmetric array of vortex-antivortex (VA) pairs, similar to a von Kármán vortex street is visible for  $S/P = 0.1$  and  $0.4$ , respectively. A soliton pair is indeed unstable in this regime [25] against modulational “snake” instability. It therefore breaks into the observed VA chain. In free space, these chains would dynamically evolve [26] to eventually disappear. Remarkably, the presence of the confining potential allows to freeze the snake structures and to easily observe them in a steady state CW experiment.

The healing length of the fluid  $\xi$  sets the dark soliton width and the vortex core size. It also naturally sets the spatial period at which the instability develops along the main channel axis [25] and therefore the number of VA pairs which appear in a channel of a finite length  $L$ .

**Conclusion.** – In this article we have reviewed our recent results on the polariton optical bistability and its related properties. By implementing the theoretical proposal [12] we demonstrated the possibility to use the bistability of the polariton system under resonant pumping together with a pump-support configuration to sustain topological excitations such as quantized vortices and dark solitons [13,19] over hundreds of microns, greatly enhancing their propagation length compared to the previous observations [6]. This experiment also revealed a very unexpected behaviour of the dark solitons: the presence of the driving field imposed by the bistable pump compensates the dark solitons repulsion as usually observed in an undriven system [6,27]. In this new configuration, dark solitons align to each other and propagate parallel.

Moreover, to achieve a full control on the formation of the topological excitations we developed a new all-optical



imprinting method by accurately shaping the excitation beam with a Spatial Light Modulator, and we managed to generate on demand dark soliton molecules on a polariton fluid [21].

Finally, we generated solitonic structures in guided low-density channel in a static polariton fluid [25] and observed their breaking into vortex streets due to transverse snake instabilities [22] showing that the flexibility of the imprinting method opens the way to deeper studies of quantum turbulence phenomena.

\*\*\*

This work has been supported by the French ANR grants (“C-FLigHT” 138678 and “QFL”, ANR-16-CE30-0021), from the ANR program “Investissements d’Avenir” through the IDEX-ISITE initiative 16-IDEX-0001 (CAP 20-25), from Region île-de-France in the framework of DIM SIRTEQ, from the European Union Horizon 2020 research and innovation program under grant agreement No. 820392 (PhoQuS). QG, AB, and DS thank the Institut Universitaire de France (IUF) for support. SK and DS acknowledge the support from the Ministry of Education and Science of the Russian Federation (0791-2020-0006).

## REFERENCES

- [1] KAVOKIN A. V., BAUMBERG J. J., MALPUECH G. and LAUSSY F. P., *Microcavities* (Oxford University Press) 2007.
- [2] CARUSOTTO I. and CIUTI C., *Rev. Mod. Phys.*, **85** (2013) 299.
- [3] AMO A., LEFRÈRE J., PIGEON S., ADRADOS C., CIUTI C., CARUSOTTO I., HOUDRÉ R., GIACOBINO E. and BRAMATI A., *Nat. Phys.*, **5** (2009) 805.
- [4] AMO A., SANVITTO D., LAUSSY F. P., BALLARINI D., VALLE E. D., MARTIN M. D., LEMAÎTRE A., BLOCH J., KRIZHANOVSKII D. N., SKOLNICK M. S., TEJEDOR C. and VIÑA L., *Nature*, **457** (2009) 291.
- [5] GROSSO G., NARDIN G., MORIER-GENOUD F., LÉGER Y. and DEVEAUD-PLÉDRAN B., *Phys. Rev. Lett.*, **107** (2011) 245301.
- [6] AMO A., PIGEON S., SANVITTO D., SALA V. G., HIVET R., CARUSOTTO I., PISANELLO F., LEMENAGER G., HOUDRE R., GIACOBINO E., CIUTI C. and BRAMATI A., *Science*, **332** (2011) 1167.
- [7] ROUMPOS G., FRASER M. D., LÖFFLER A., HÖFLING S., FORCHEL A. and YAMAMOTO Y., *Nat. Phys.*, **7** (2011) 129.
- [8] NARDIN G., GROSSO G., LÉGER Y., PIETKA B., MORIER-GENOUD F. and DEVEAUD-PLÉDRAN B., *Nat. Phys.*, **7** (2011) 635.
- [9] LERARIO G., FIERAMOSCA A., BARACHATI F., BALLARINI D., DASKALAKIS K. S., DOMINICI L., DE GIORGI M., MAIER S. A., GIGLI G., KÉNA-COHEN S. and SANVITTO D., *Nat. Phys.*, **13** (2017) 837.
- [10] KIVSHAR Y. S. and PELINOVSKY D. E., *Phys. Rep.*, **331** (2000) 117.
- [11] CIUTI C. and CARUSOTTO I., *Phys. Status Solidi (b)*, **242** (2005) 2224.
- [12] PIGEON S. and BRAMATI A., *New J. Phys.*, **19** (2017) 095004.
- [13] LERARIO G., MAÎTRE A., BODDEDA R., GLORIEUX Q., GIACOBINO E., PIGEON S. and BRAMATI A., *Phys. Rev. Res.*, **2** (2020) 023049.
- [14] BOULIER T., TERÇAS H., SOLNYSHKOV D., GLORIEUX Q., GIACOBINO E., MALPUECH G. and BRAMATI A., *Sci. Rep.*, **5** (2015) 1.
- [15] BOULIER T., CANCELLIERI E., SANGOUARD N. D., GLORIEUX Q., KAVOKIN A., WHITTAKER D. M., GIACOBINO E. and BRAMATI A., *Phys. Rev. Lett.*, **116** (2016) 116402.
- [16] PIGEON S., CARUSOTTO I. and CIUTI C., *Phys. Rev. B*, **83** (2011) 144513.
- [17] HOUDRÉ R., WEISBUCH C., STANLEY R. P., OESTERLE U. and ILEGEMS M., *Phys. Rev. B*, **61** (2000) R13333.
- [18] AMO A., PIGEON S., ADRADOS C., HOUDRÉ R., GIACOBINO E., CIUTI C. and BRAMATI A., *Phys. Rev. B*, **82** (2010) 081301.
- [19] LERARIO G., KONIAKHIN S. V., MAÎTRE A., SOLNYSHKOV D., ZILIO A., GLORIEUX Q., MALPUECH G., GIACOBINO E., PIGEON S. and BRAMATI A., *Phys. Rev. Res.*, **2** (2020) 042041.
- [20] ZAKHAROV V. and SHABAT A., *Sov. J. Exp. Theor. Phys.*, **37** (1973) 823.
- [21] MAÎTRE A., LERARIO G., MEDEIROS A., CLAUDE F., GLORIEUX Q., GIACOBINO E., PIGEON S. and BRAMATI A., *Phys. Rev. X*, **10** (2020) 041028.
- [22] CLAUDE F., KONIAKHIN S. V., MAÎTRE A., PIGEON S., LERARIO G., STUPIN D. D., GLORIEUX Q., GIACOBINO E., SOLNYSHKOV D., MALPUECH G. and BRAMATI A., *Optica*, **7** (2020) 1660.
- [23] KAMCHATNOV A. M. and PITAEVSKII L. P., *Phys. Rev. Lett.*, **100** (2008) 160402.
- [24] KWON W. J., KIM J. H., SEO S. W. and SHIN Y.-I., *Phys. Rev. Lett.*, **117** (2016) 245301.
- [25] KONIAKHIN S. V., BLEU O., STUPIN D. D., PIGEON S., MAITRE A., CLAUDE F., LERARIO G., GLORIEUX Q., BRAMATI A., SOLNYSHKOV D. and MALPUECH G., *Phys. Rev. Lett.*, **123** (2019) 215301.
- [26] DUTTON Z., BUDDE M., SLOWE C. and VESTERGAARD HAU L., *Science*, **293** (2001) 663.
- [27] HIVET R., FLAYAC H., SOLNYSHKOV D. D., TANESE D., BOULIER T., ANDREOLI D., GIACOBINO E., BLOCH J., BRAMATI A., MALPUECH G. and AMO A., *Nat. Phys.*, **8** (2012) 724.